Weakened Flow, Persistent Circulation, and Prolonged Weather Extremes in Boreal Summer: Patterns and Mechanisms

Chapter · June 2017

DOI: 10.1002/9781119068020.ch4

4 authors, including:

Dim Coumou
Potsdam Institute for Climate Impact Research
99 PUBLICATIONS **3,490** CITATIONS

SEE PROFILE

Kai Kornhuber
University of Oxford
24 PUBLICATIONS **245** CITATIONS

SEE PROFILE

Jascha Lehmann
Potsdam Institute for Climate Impact Research
23 PUBLICATIONS **369** CITATIONS

SEE PROFILE

4

Weakened Flow, Persistent Circulation, and Prolonged Weather Extremes in Boreal Summer

Dim Coumou[1], Kai Kornhuber[2], Jascha Lehmann[2], and Vladimir Petoukhov[1]

ABSTRACT

Changes in atmospheric circulation can strongly alter the frequency and/or magnitude of high-impact extreme weather events. Here we address the link between circulation changes and the occurrence of long-lasting heat waves in the Northern Hemisphere summer. We show that boreal summer circulation has seen pronounced changes in circulation over the last decades, possibly related to rapid warming of the Arctic. Generally, the mid-latitude zonal mean flow has weakened and also the kinetic energy associated with transient synoptic eddies has reduced. At the same time, for some wave numbers, we see an increased occurrence-frequency of high-amplitude quasi-stationary waves. We argue that this increase in frequency is associated with a recent cluster of resonance events that can create such high-amplitude waves. The reduction in amplitude of fast-moving transient waves and the more-frequent occurrence of high-amplitude quasi-stationary waves both favor more persistent weather conditions. We present statistical evidence of links between such persistent upper-level flow and the occurrence of heat extremes at the surface.

4.1. INTRODUCTION

4.1.1. Detected Changes in Midlatitude Summer Circulation

The Northern Hemisphere midlatitudes have seen significant changes in the large-scale summer circulation over the last decades [*Overland et al.,* 2012; *Francis and Vavrus,* 2015; *Coumou et al.*, 2015]. The zonal mean zonal wind (or "jet") has weakened by about 5% (see Fig. 4.1), a signal that is seen in different reanalysis products and at different pressure levels [*Coumou et al.*, 2015]. The driver behind this weakening might be the much faster warming in the Arctic as compared to the rest of the hemisphere, a phenomenon known as Arctic amplification (Fig. 4.2; see also Chapter 2). This reduces the pole-to-equator temperature gradient and thereby the thermally driven jet (top panel Fig. 4.1). However, a strict direction of causality has not been shown. In principle it could be the other way around, too, whereby a change in midlatitude circulation alters the poleward heat transport, which would give rise to more rapid warming in the Arctic [*Cohen et al.*, 2014; *Walsh*, 2014]. For example, an alternative hypothesis has been proposed where the warmer Arctic is a consequence of midlatitude circulation changes, which would increase the exchanges of cold air from the Arctic with warmer air from lower latitudes, triggered by teleconnections originating from the tropical Pacific [*Trenberth et al.*, 2014; *Palmer,* 2014]. Irrespective of the underlying drivers, changes in midlatitude circulation are expected to affect day-to-day weather variability and possibly extreme weather events.

[1] *Institute for Environmental Studies (IVM), Department of Water and Climate Risk, VU University Amsterdam, Amsterdam, The Netherlands; Potsdam Institute for Climate Impact Research, Earth System Analysis, Potsdam, Germany*

[2] *Potsdam Institute for Climate Impact Research, Earth System Analysis, University of Potsdam, Faculty of Science, Potsdam, Germany*

Climate Extremes: Patterns and Mechanisms, Geophysical Monograph 226, First Edition.
Edited by S.-Y. Simon Wang, Jin-Ho Yoon, Christopher C. Funk, and Robert R. Gillies.

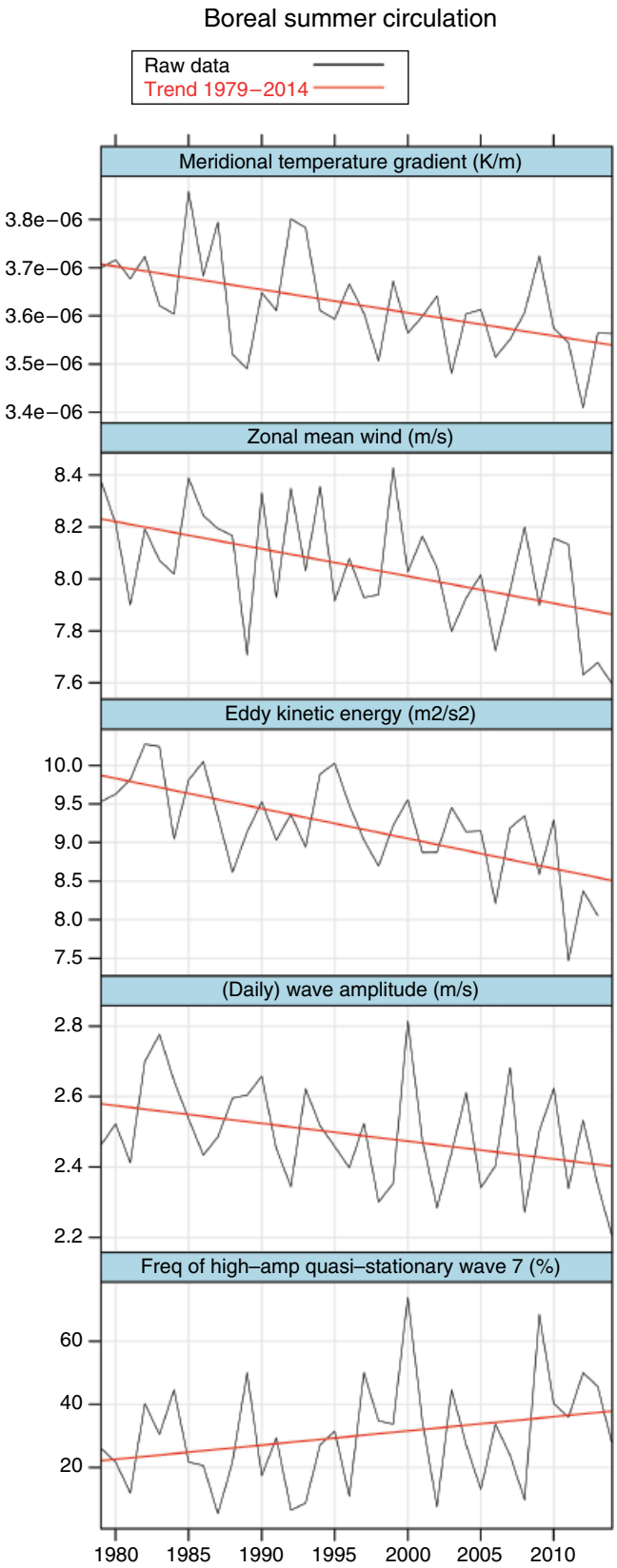

In conjunction with the summer jet, the kinetic energy associated with transient synoptic-scale weather systems has seen a significant weakening as well [*Coumou et al.*, 2015]. This kinetic energy can for example be extracted by bandpass filtering daily wind field data, because synoptic activity has typical timescales of 2 to 5 days, bringing weather variability on subweekly timescales. Typical wave lengths of synoptic transients are of the order of 2000–3500 km, or wave numbers from 6 to 10, with relatively fast phase speeds (i.e., eastward propagation) of the order of 6–12 m/s. These waves are *free* waves in the sense that they do not require any forcing but are a direct product of the atmospheric instability in the midlatitudes. Thus, in the absence of any temperature or orographic forcing, as for example on a so-called aquaplanet, these waves would still emerge [*Schneider et al.*, 2014]. Based on linear Rossby wave theory, one would expect the phase speed of these waves to become smaller under a weakened background flow. Starting from the linearized nondivergent barotropic vorticity equation [*Pedlosky,* 1979] without any thermal or orographic forcing (i.e., an equation describing adiabatic free atmospheric waves), an equation for the phase speed c can be derived:

$$c = U - \frac{\beta}{\left(k^2 + l^2\right)} \tag{4.1}$$

where U denotes the zonal mean zonal wind, β the Rossby parameter, and k and l, respectively, the zonal and meridional wave numbers. Thus, these *free* waves essentially flow on top of the background flow (U) and a weakening of the latter results in slower phase speeds. However, so far, no robust changes in phase speed have been detected in the observations. In contrast, significant trends have

Figure 4.1 Weakening summer circulation in the Northern Hemisphere midlatitudes over 1979–2014. Absolute changes in meridional temperature gradient, zonal mean wind, eddy kinetic energy (EKE), daily wave amplitudes for waves 6–10, and frequency of high-amplitude quasi-stationary wave 7. Variables are based on ERA-interim reanalysis, calculated at 500 mb, averaged over 35°N–65°N and all longitudes, for June-July-August. Plotted are actual observations and the linear trend, which are all significant at 95% confidence except for the linear trend in the bottom panel, which is significant at 90% confidence only. Similar trends are found at other pressure levels and in other reanalyses [*Coumou et al.*, 2014, 2015]. *See electronic version for color representation.*

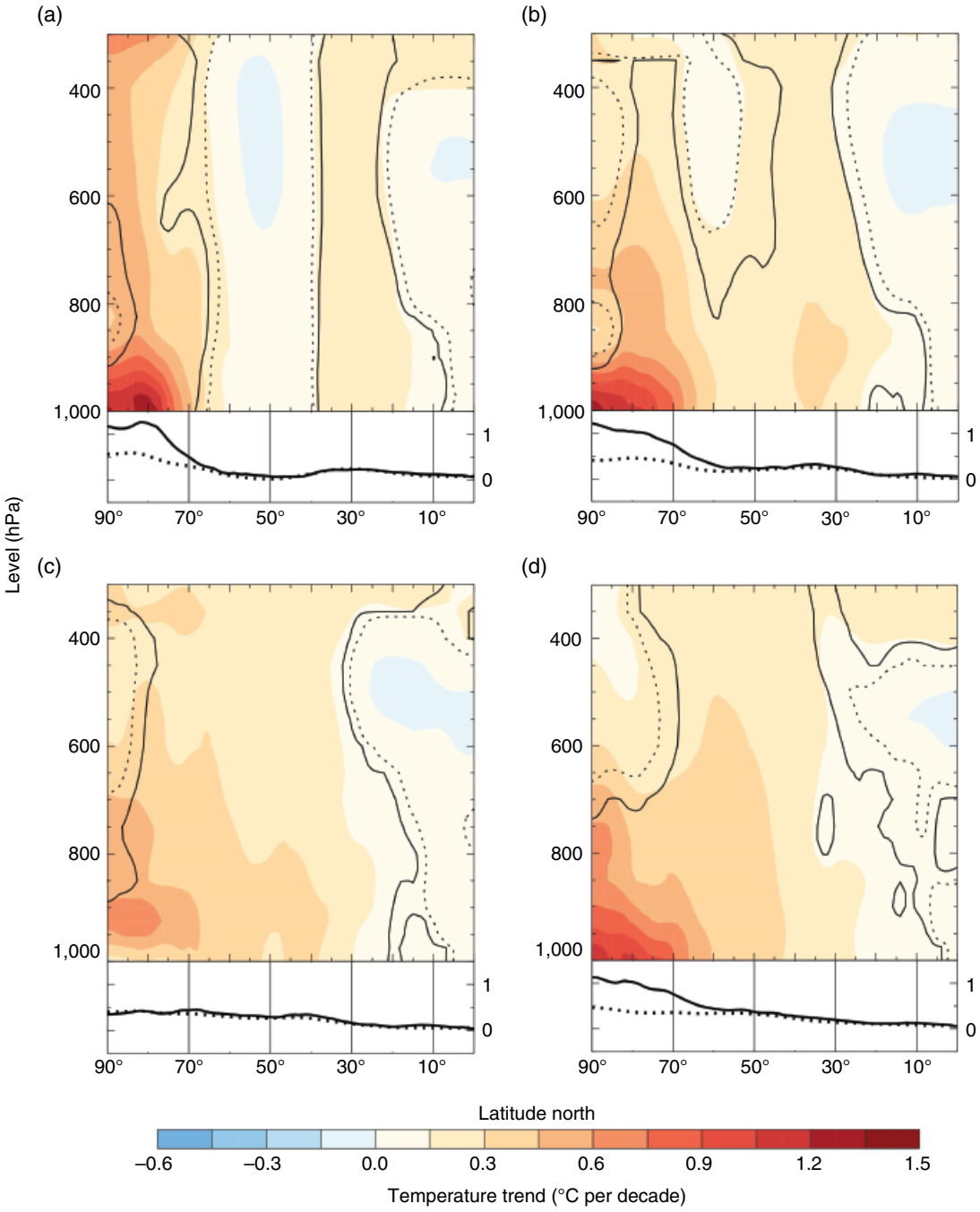

Figure 4.2 Arctic amplification of temperature trends over 1979–2014 for each season. Trends in zonal mean temperature for (a) winter (December–February), (b) spring (March–May), (c) summer (June–August), and (d) autumn (September–November) based on the ERA-interim reanalysis. Black contours indicate regions with significance at the 99% (solid lines) and 95% (dotted lines) confidence levels. The line graphs show trends averaged over the lower atmosphere (950–1000 hPa; solid lines) and over the entire atmospheric column (300–1000 hPa; dotted lines). From *Cohen et al.* [2014].

been detected in the amplitude of these waves, defined as the magnitude of the north-south flow (meridional wind in units of m/s). Amplitudes are expected to decline when the jet weakens, which can be derived from theoretical considerations [*Coumou et al.*, 2011]. This behavior is also seen in numerical experiments of both idealized general circulation models (GCMs) and comprehensive GCMs [*Schneider et al.*, 2014]. In general, transient eddies are forced by the jet via vertical shear (and thus baroclinicity) but can also accelerate it via the eddy-driven jet [*Woollings and Blackburn*, 2012; *Cohen et al.*, 2014; *Lehmann et al.*, 2014]. Thus, a weakening of the jet is expected to weaken synoptic eddy activity, in agreement with the observed long-term trends. As shown in Figure 4.1, statistically significant reductions are seen in both the mean amplitude of wave numbers 6–10 as well as in the total kinetic energy associated with synoptic eddies (eddy kinetic energy, or EKE). This summertime weakening of both the jet and EKE is also a very robust signal in future projections of CMIP5 climate models [*O'Gorman*, 2010; *Lehmann et al.*, 2014].

In addition to free waves, orography and thermal anomalies (like land-ocean temperature contrasts) generate *forced* waves in the midlatitudes. Since the forcing patterns change on substantially longer timescales of several weeks, these waves can be considered quasi-stationary. Due to the large-scale nature of the forcing patterns, forced waves tend to have smaller wave numbers (<6). The forced-component (and therefore also the quasi-stationary component) of wave numbers 6–10 is normally small. Note that free waves can also be quasi-stationary when the second term in equation (4.1) is similar in magnitude as the zonal mean jet (U), which is normally the case for wave 4. Thus, in general, the low wave number regime of the flow is quite different from the high wave number regime, with the latter dominated by fast moving waves. Only when averaging over longer time spans, like 15 days to monthly means, one effectively removes this transient wave component and the quasi-stationary component remains. For waves 6–10, this quasi-stationary component has generally a low magnitude and also little significant trends can be detected. Nevertheless, the trend in the highest amplitudes of the quasi-stationary component of wave 7 is upward. The lowest panel of Figure 4.1 plots how often the seventieth percentile wave-amplitude in 15-day running mean wind field data is exceeded, showing a moderate upward trend. This is also consistent with the reported increase in frequency of high-amplitude, quasi-stationary wave 7 [*Coumou et al.*, 2014]. Though this signal is seen in different reanalyses and at different pressure levels [*Coumou et al.*, 2014], it should be noted that statistically it is only marginally significant [*Wang et al.*, 2013]. Nevertheless, it is consistent with the recent cluster of resonance events involving wave 7 as discussed later.

In summary, we can conclude that boreal summer circulation has changed in three important ways over the last decades: (1) A weakening of the zonal mean jet, (2) a reduction in fast-moving synoptic wave activity and (3) a (marginally significant) increase in frequency of the occurrence of high-amplitude quasi-stationary wave 7. These three detectable changes all point at more persistent circulation patterns.

4.1.2. Midlatitude Rossby Waves and Extreme Weather

In general, persistent circulation patterns can lead to extreme weather and in particular to prolonged heat waves in summer. Slow wave propagation prolongs the prevailing weather conditions at the surface and can therefore lead to extremes on timescales of weeks: One day with temperatures over 30°C in western Europe is not unusual, but 10 or 20 days in a row will be. It has been demonstrated that high-amplitude quasi-stationary waves in the atmosphere are statistically linked to extreme weather at the surface [*Screen and Simmonds,* 2014; *Coumou et al.*, 2014]. Especially regions at the western boundary of the continents like the western United States [*Wang et al.*, 2010] or Europe show the strongest association between surface extremes and upper-level waves. Here, moderate temperatures tend to be associated with reduced quasi-stationary wave amplitudes and extreme temperatures with amplified quasi-stationary waves [*Screen and Simmonds*, 2014].

In contrast, strong transient wave activity, as captured by EKE, is linked to moderate surface temperatures and vice versa [*Coumou et al.*, 2015; *Lehmann and Coumou*, 2015]. Over most continental regions affected by storm tracks, there is a significant negative correlation between monthly EKE and surface temperature (Fig. 4.3). Thus, the hottest summers are associated with extremely low EKE, while mild summers are associated with more pronounced EKE. Again the western boundaries of the continents, notably Europe, are especially sensitive but also the eastern United States and western Asia. This makes sense as these regions are most directly influenced by the storm tracks. If EKE is low, this implies that weather variability on 2–5 day timescales is low, which is consistent with blocking anticyclones associated with quasi-stationary waves. In summer, transient waves transport moist and cool air from the oceans to the continents bringing relief during periods of oppressive heat [*Kyselý and Huth*, 2005; *Kyselý,* 2008]. Thus, low transient wave activity implies that cool maritime air masses become less frequent creating favorable conditions for blocking anticyclonic flow over continents and the buildup of heat and drought conditions. Amplifying local feedback mechanisms, such as soil-moisture feedbacks, can further drive temperatures upward, inhibit cloud formation, and

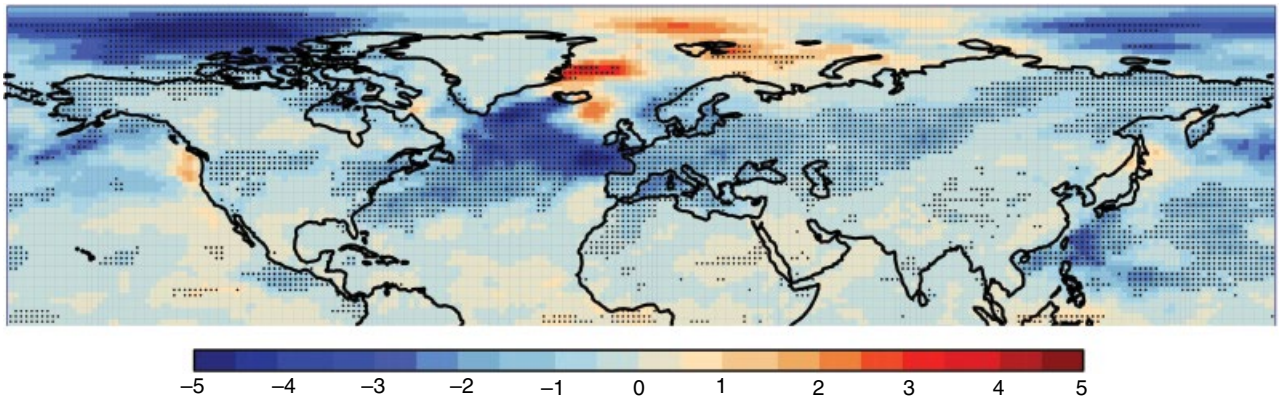

Figure 4.3 Regression slope between EKE and near-surface temperature in summer months (June–August) in units of m^2s^{-2}/K. Both variables were calculated from ERA-interim data and linearly detrended at each grid point. Significant negative correlation (stippling indicating 95% confidence) exists over most storm-track–affected regions. From *Coumou et al.* [2015].

thereby enhance the anticyclonic flow over the continents [*Schär et al.*, 2004; *Alexander*, 2010; *Mueller and Seneviratne*, 2012]. Thus, an absence of substantial transient wave activity likely prolongs the duration of blocking weather systems, as for example during the Russian heat wave of 2010. The record-breaking July temperatures over Moscow in that year were associated with extremely low EKE [*Coumou et al.*, 2015].

In summary, the observed trends in boreal summer circulation (Fig. 4.1) favor more persistent weather in summer and hence heat extremes on timescales of several weeks.

4.2. RESONANT CIRCULATION REGIMES

The observed reduction in transient wave activity seems to be a direct response of the weakening jet. Climate models project both summer jet and EKE to weaken under future high-emission scenarios and the projected relative changes in these quantities are consistent with those observed [*Coumou et al.*, 2015]. However, the observed increase in frequency of high-amplitude quasi-stationary wave 7 cannot be directly linked to the weakening jet.

To explain this increased frequency, a highly nonlinear, dynamical mechanism is invoked: resonance. This mechanism, which was first proposed by *Petoukhov et al.* [2013], can amplify the quasi-stationary component of waves 6, 7, or 8. As stated above, these wave numbers normally have a fast eastward propagation and their quasi-stationary component tends to be weak. Forcing of these waves is normally weak in the midlatitudes and their energy is effectively dispersed toward the poles and equator. However, under specific conditions, their wave energy can be trapped in midlatitudinal waveguides, with only weak dispersion at the lateral boundaries. If this happens and if the forcing for the trapped wave is large enough, then resonance can strongly magnify the wave amplitude. There are thus two important criteria that need to be fulfilled for resonance to occur: (1) waveguide formation, which traps the energy of wave 6, 7, or 8 in the midlatitudes, and (2) reasonably large forcing of the trapped free wave.

4.2.1. Waveguide

The jet stream can guide waves in the zonal direction and thereby trap them inside the midlatitudes. Whether a particular wave is trapped depends on the shape of the zonal mean zonal wind (U) and the wave number itself (k). Based on the linearized stationary barotropic vorticity equation at the equivalent barotropic level (in the mid/upper troposphere at about 300–500 hPa), an expression for the square of the meridional wavenumber of the trapped wave (l^2) can be derived [*Petoukhov et al.*, 2013]:

$$l^2(U,k,\varphi)=\frac{2\Omega cos^3\varphi}{aU}-\frac{cos^2\varphi}{a^2U}\frac{d^2U}{d\varphi^2}+\frac{sin\varphi cos\varphi}{a^2U}\frac{dU}{d\varphi}+\frac{1}{a^2}-\left(\frac{k}{a}\right)^2 \tag{4.2}$$

Here a is the Earth's radius, Ω its angular velocity, and φ latitude. Note that l may be a real or purely imaginary number and thus l^2 can change sign. For a waveguide to form for wave number k, two turning points are needed at two sufficiently distant latitudinal locations. At these turning points, the energy of wave k gets reflected back toward the midlatitudes. For this to occur, l^2 has to be positive inside the waveguide and change sign at the turning points themselves while U has to be positive (i.e., eastward) inside and directly outside the waveguide. The latter is normally the case outside the tropics and thus it is especially the change in sign of l^2 that is important. Finally, the turning points have to be located

at a sufficiently large distance (several degrees latitude) so that the waveguide exceeds the characteristic scale of the relevant Airy function, which governs the latitudinal boundary conditions of the waveguide [*Petoukhov et al.*, 2013].

4.2.2. Wave Forcing

Trapping of a quasi-stationary free wave in a midlatitude waveguide not necessary leads to amplification of that wave: Forcing is needed as well. When a waveguide exists for a synoptic wave with wavenumber k the following approximate equation for the amplitude of the forced quasi-stationary component is valid [*Petoukhov et al.*, 2013]:

$$A_m = \frac{A_{m,F}}{\sqrt{\left[\left(\frac{k}{a}\right)^2 - \left(\frac{m}{a}\right)^2\right]^2 + \left(\frac{L}{a^2} + \frac{R_0^2}{L}\right)^2 \left(\frac{m}{a}\right)^2}} \quad (4.3)$$

Here R_0 is the Rossby number for eddies and L is the characteristic Rossby radius, which are both taken as constants. $A_{m,F}$ is the amplitude of the forcing at the equivalent barotropic level (in units of m/s) for wavenumber m, and is a function of temperature and orography. Equation (4.3) shows that when k is close to m (i.e., when the forcing pattern is close to that of the trapped free wave), the denominator becomes small and thus A_m large. This is the essence of resonant amplification. Note that the forcing $A_{m,F}$ can thus be moderate (although not zero) for resonance and hence high wave amplitudes to occur.

4.2.3. Resonance Occurrence

Based upon the above described criteria, resonance events in the Northern Hemisphere have been identified to occur primarily in summer and also spring when the background flow is relatively weak. In these seasons, so-called double jet flow configurations, characterized by two peaks in the zonal mean zonal wind, are much more likely to occur. Such double jet states favor waveguide formation due to the unusual shape of the zonal mean zonal wind across latitudes, which primarily determines l^2. From the thermal wind equation it follows that in order to generate double jet states, sharp poleward temperature gradients are needed at mid (~45°N) and subpolar (~70°N) latitudes with weaker gradients in between. Weak thermal gradients around 50°N–65°N are unlikely to occur in winter and autumn when the equator to pole temperature difference is much larger. This is likely the underlying reason that double jet states and hence resonance events are limited to summer and spring, when the overall equator to pole temperature drop is much more moderate. Likewise, the cluster of resonance events in recent summers (see section 4.3.2, Cluster of Resonance Events) might thus be related to the significant reduction in the meridional temperature gradient around 50°N over the last decades (Fig. 4.1).

4.3. REAL EVENTS

4.3.1. Case Study: Summer 2010

The summer of 2010 saw anomalous large-scale flow patterns over the Eurasian continent, which has been identified as a key factor behind both the Russian heat wave and Pakistan flooding that summer [*Schubert et al.*, 2011; *Schneidereit et al.*, 2012; *Lau and Kim*, 2012; *Tachibana et al.*, 2010; *Petoukhov et al.*, 2013; *Schubert et al.*, 2014]. These extreme events illustrated how destructive extreme weather can be to societies: The death toll in Moscow has been estimated at 11,000 and drought-caused grain-harvest losses of 30%, leading to a Russian export ban on wheat [*Coumou and Rahmstorf*, 2012]. At the same time Pakistan was hit by the worst flooding in its history, which affected approximately one-fifth of its total land area and 20 million people [*Hong et al.*, 2011; *Coumou and Rahmstorf*, 2012]. The heat wave over western Russia was due to a blocking high, which resulted in record temperatures exceeding the extreme European heat wave of 2003 in amplitude and spatial extent [*Dole et al.*, 2011; *Rahmstorf and Coumou*, 2011; *Barriopedro et al.*, 2011]. In fact, based upon a global heat wave index, the event was quantified as the strongest heat wave ever [*Russo et al.*, 2014]. Especially striking was the long lifetime of the blocking event: Roughly 30% of summer days in western Russia were considered as blocking days where normally this is only about 10% [*Schneidereit et al.*, 2012]. The anticyclonic flow anomaly was associated with a stationary Rossby wave train extending over the full Eurasian continent and beyond. In fact, several studies have highlighted the hemispheric nature of these flow anomalies [*Tachibana et al.*, 2010; *Schubert et al.*, 2011; *Petoukhov et al.*, 2013]. The trough downstream of the western Russia anticyclone was instrumental in triggering anomalously heavy rainfall over northern Pakistan leading to flooding of the Indus River [*Lau and Kim*, 2012].

Figure 4.4 shows Hovmöller diagrams of a set of zonal mean dynamic variables during the summer of 2010 over the Northern Hemisphere. In early July, a pronounced second peak in the zonal mean zonal wind emerges at about 70°N creating a clear double jet flow configuration, which persists until half of August (Fig. 4.4a). This shift in the zonal mean flow regime is associated with a pronounced warming of regions around 60°N, that is, the approximate latitude of Moscow. In fact, in the single jet regime (June and late August), pronounced positive temperature anomalies are seen over the Arctic Ocean (North

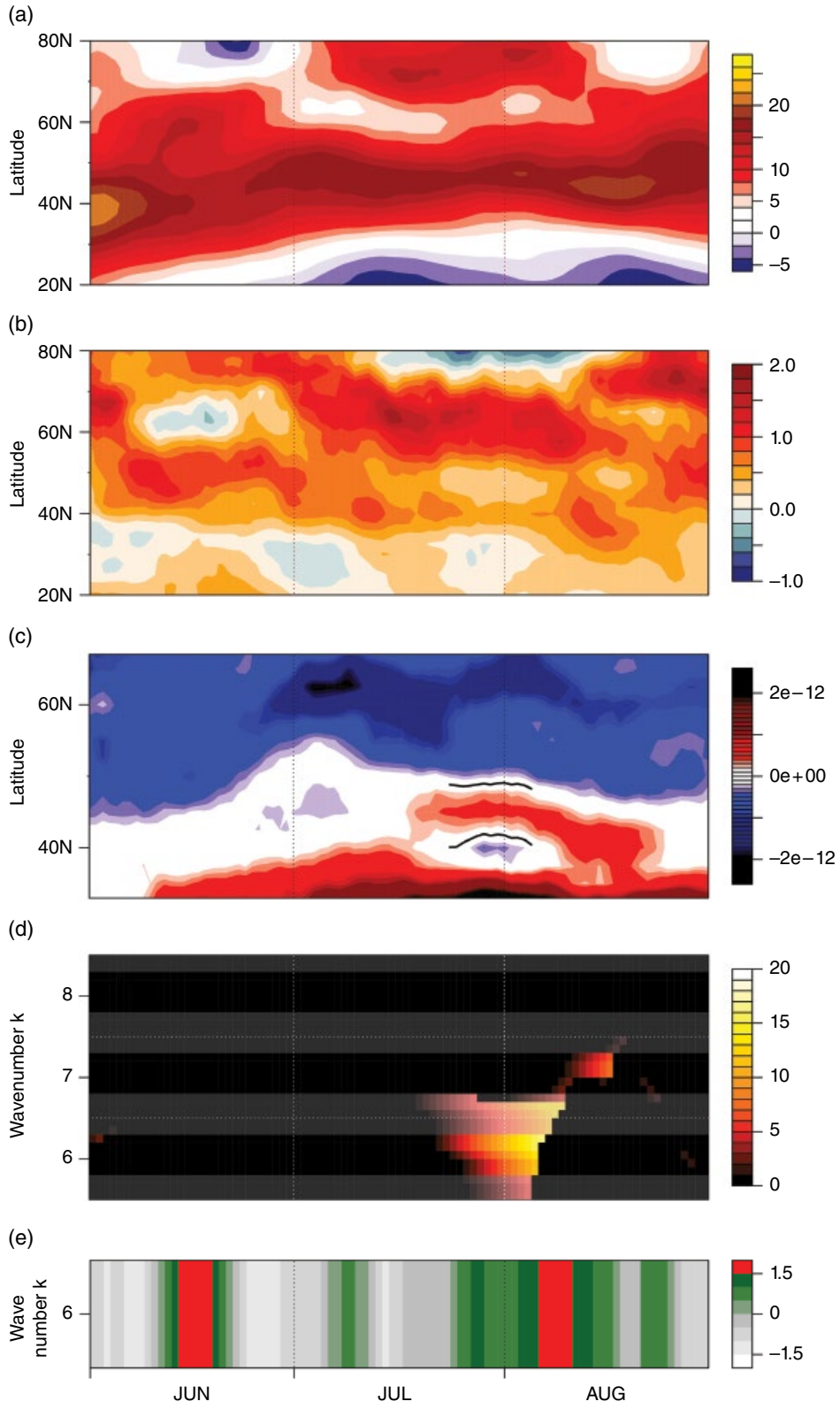

Figure 4.4 Double jet and resonant amplification during summer of 2010. Northern Hemisphere Hovmöller diagrams during summer 2010 for (a) zonal wind, (b) temperature anomaly, and (c) $I^2(k=6)$. Variables are calculated from the ERA-interim reanalysis using a 15 day running mean low-frequency bandpass filter and averaged over all longitudes. Temperature anomalies from climatology (panel b) were calculated at each grid point before averaging over all longitudes. The black lines in panel (c) indicate the emergence of the two turning points of the waveguide for wave 6. Panel (d) plots the number of consecutive days for which resonance conditions were fulfilled for waves 6–8, and panel (e) plots the observed amplitude of wave 6. (*See insert for color representation of the figure.*)

of ~70°N) and further south (between 40°–50°N), while in the double jet regime they are concentrated around 60°N (Fig. 4.4b). The zonal mean flow changes result in the formation of a waveguide by mid-July, which becomes pronounced in late July and early August (Fig. 4.4c). Two turning points can be distinguished in Figure 4.4c: one at 40°N and one at about 50°N (solid black lines), that is, placed roughly in between the latitudes of the heat wave in Moscow and the flooding in Pakistan. Following the criteria defined above, l^2 is positive between those latitudes and changes sign at the turning points themselves. Further, the zonal mean flow is clearly positive over all latitudes north of about 30°N including the position of the waveguide. In addition, the turning points are located at sufficiently large distance and thus all criteria for a waveguide trapping waves with wave numbers close to 6 in the midlatitudes were fulfilled. Since also the forcing A_F for wave 6 was sufficiently large (see equation [4.3]), the trapped wave underwent resonant amplification (Fig. 4.4d). This amplification of wave 6 is also observed: It starts by mid-July when the waveguide is first detected and maximum amplitudes are reached in early August (red in Fig. 4.4e). This panel also shows that in mid-June similarly high wave amplitudes are observed which were not related to the resonance mechanism, highlighting that of course other mechanisms can also cause high-amplitude waves.

This analysis, and more detailed analyses described in [*Petoukhov et al.*, 2013], illustrate that resonance played an important role in creating high-amplitude quasi-stationary Rossby waves from mid-July to early August 2010, which was the most severe period of the Russian heat wave and which includes the period of flooding in Pakistan.

4.3.2. Cluster of Resonance Events

Based upon the criteria discussed above and analyzing monthly data for July and August, *Petoukhov et al.* [2013] identified 19 resonance months since 1980 (Fig. 4.5). Many of these months were associated with memorable extreme weather events, including severe heat waves and flooding events in Europe and heat waves and droughts in the United States. Coinciding with the onset of rapid Arctic amplification in 2000, there appears to be a cluster of resonance events though its significance cannot be assessed. Nevertheless, in the post-2000 period, the frequency of July or August resonance months has almost doubled compared to the pre-2000 period. Especially, resonance involving waves 7 and 8 seems to have occurred more frequently recently. Spectral analysis of daily data of July and August days, *Coumou et al.* [2014] showed that there indeed have been significant changes with more frequent high-amplitude quasi-stationary waves with these wave numbers. In the post-2000 period, the number of days with a quasi-stationary wave 7 with amplitudes larger than 3 m/s increased by 30%, and, with amplitudes larger than 5 m/s, have more than doubled [*Coumou et al.*,

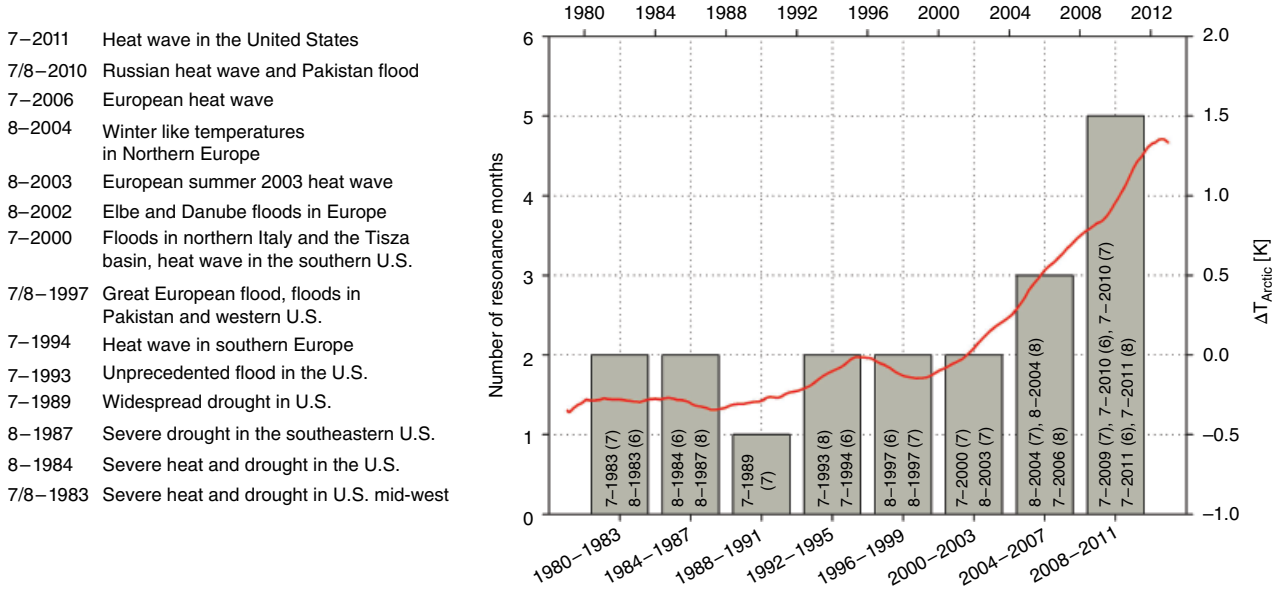

Figure 4.5 Number of identified July and August resonance events [*Petoukhov et al.,* 2013] binned together in 4 yr periods from 1980 to 2011. Text in the grey bars indicates the actual months and wave numbers involved (in brackets) and the table on the left lists the associated extreme weather events. The red line plots the difference in surface warming in the Arctic (north of 65°N) and in the rest of the Northern Hemisphere (south of 65°N), based upon the temperature dataset by *Cowtan and Way* [2013]. From *Coumou et al.* [2014]. *See electronic version for color representation.*

2014]. These findings are also consistent with the independent analysis as plotted in the lowest panel of Figure 4.1. This shows a moderate upward trend in the occurrence-frequency of a quasi-stationary wave 7 with an amplitude exceeding the seventieth percentile. This threshold is somewhat subjective and the upward trend is only marginally significant and thus this finding should be treated with caution. It nevertheless is consistent with the cluster analysis presented in *Coumou et al.* [2014]. We thus argue that the recent cluster of resonance events has led to a detectable increase in the overall frequency of high-amplitude quasi-stationary wave 7 since 2000. This occurred while transient wave activity, best captured by EKE, declined pronouncedly.

4.3.3. Statistics of Resonance Events

Based on the resonance periods identified by *Petoukhov et al.* [2013], *Coumou et al.* [2014] performed statistical analysis to quantify how anomalous upper-level wind fields and surface weather were during resonance events. To determine upper-level wave activity, spectral analysis of the 500 mb and 300 mb daily meridional wind field over a midlatitudinal belt stretching from 35°N to 65°N were performed using both the ERA-interim [*Dee et al.*, 2011] and NCEP-NCAR [*Kalnay et al.*, 1996] reanalyses. Since the meridional wind field was analyzed, wave amplitudes reflect actual north-south wind speeds. Further, also phase-speed and the daily zonal mean zonal wind in this midlatitudinal belt were extracted [*Coumou et al.*, 2014]. Figure 4.6 summarizes the key findings of these analyses presented as 2D probability density plots of phase-speed with respect to wave amplitude (top panels) and zonal mean wind (bottom panels) for waves 6 (left panels), 7 (middle panels), and 8 (right panels). The July-August climatological mean (solid curves) shows that the wave spectrum is dominated by eastward traveling waves (positive phase speed) with the speed increasing with wave number, as predicted by linear Rossby wave theory (equation [4.1]). Still, especially for waves 6 and 7, a sizeable proportion of the probability density distribution is associated with quasi-stationary waves (with an absolute phase speed c less than ~2 m/s) or with westward propagating waves. However, these slow moving waves

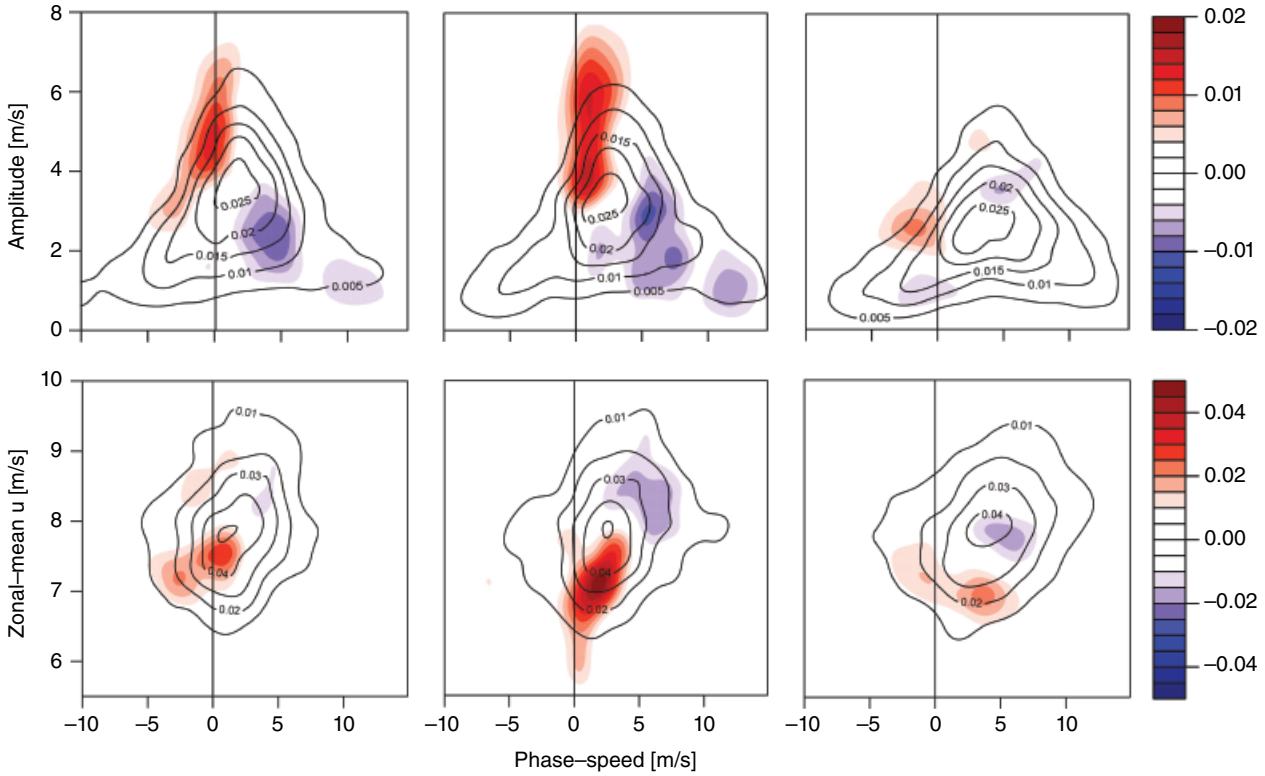

Figure 4.6 2D probability density distributions for daily values of phase speed (horizontal axis) against respectively (top) wave amplitude and (bottom) zonal mean zonal wind for (left) wave 6, (middle) wave 7, and (right) wave 8. Variables are based on ERA-interim reanalysis at 500 mb, averaged over 35°N–65°N for days in July–August (solid lines). Shading indicates anomalies from July-August climatology during resonance events showing increased frequencies of high-amplitude quasi-stationary waves. Adapted from *Coumou et al.* [2014]. *See electronic version for color representation.*

generally have low amplitudes. Shading in Figure 4.6 shows the anomaly in the distributions during resonance periods, showing distinct patterns. First of all, a pronounced increase in occurrence-frequency of high-amplitude quasi-stationary waves is observed, notably for waves 6 and 7. Next, the occurrence-frequency of fast-moving waves (i.e., faster than the July-August climatological mean phase speed) is substantially reduced, again most pronounced for waves 6 and 7. Further, *Coumou et al.* [2014] report that the mean phase speed during resonance periods reduces by more than a factor of two for wave 7 and by more than a factor of three for wave 6. Also distinct patterns are observed in the anomaly for the zonal mean zonal wind spectra (Fig. 4.6, bottom panels). Generally, a weakening of the zonal flow is observed, which is most pronounced for wave 7 (by roughly 5% in the mean). This weakening can thus explain some of the observed slowdown in wave propagation (following equation [4.1]) but the change is too small to fully account for the strong reduction in phase speed observed. Moreover, also the high-amplitude character of the quasi-stationary waves requires an amplification mechanism, not just a slowdown.

In a next step, it is analyzed whether surface weather conditions were also more extreme during these resonance months. To quantify this a simple midlatitudinal extreme (MEX) index is defined [*Coumou et al.*, 2014]:

$$MEX\left(x,t\right)=\frac{\left(\frac{1}{N}\sum_{i}^{N}\left(\frac{\Delta x_i\left(t\right)}{\sigma\left(x_i\right)}\right)^2-\mu_{MEX}\right)}{\sigma_{MEX}} \qquad (4.4)$$

Here x can in principle refer to any meteorological variable defined in the midlatitudes (35°N–65°N) but here we use near-surface temperature, with $\Delta x_i(t)$ its anomaly at time step t and $\sigma(x_i)$ its standard deviation at location i. The *MEX* index is normalized by subtracting its time-averaged mean (μ_{MEX}) and division by its standard deviation (σ_{MEX}) such that the climatological distribution centers around 0 and is defined in units of standard deviation [*Coumou et al.*, 2014]. If the *MEX* index has large positive values, this indicates that extreme temperatures (hot or cold) occur simultaneously in many locations throughout the midlatitudes. Combining hot and cold anomalies (by means of the square in equation [4.4]) makes sense as strong wave activity is expected to bring hot conditions in some regions and cold conditions in others [*Screen and Simmonds,* 2014].

Figure 4.7 shows probability density distributions for the *MEX* index based on daily and monthly mean surface temperatures. The July-August climatological distributions (black) are clearly asymmetric with a fat extreme tail and center around 0 (by definition). The daily heat index during resonance periods shows a statistically significant shift (p-value < 0.05) to more extremes with *MEX* indices beyond 2 standard deviations becoming much more likely. Moreover, the distribution of the monthly *MEX* index shows even more pronounced changes during resonance, with a significant shift (p-value < 0.05) toward more extremes. The very pronounced changes seen in monthly data, as compared to more moderate changes in daily data, indicates that it was especially the persistence in weather that led to extreme heat on longer, that is, monthly, timescales.

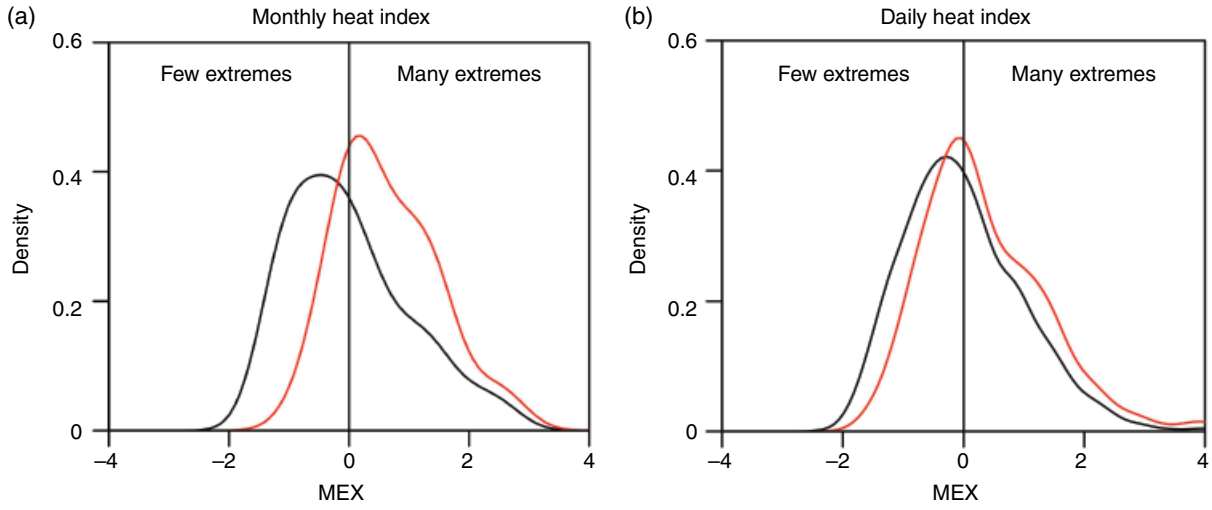

Figure 4.7 Midlatitudinal extreme index MEX (equation [4.4]) in units of standard deviation for (a) monthly heat extremes and (b) daily heat extremes for July-August climatology (black) and resonance events (gray). Adapted from *Coumou et al.* [2014]. *See electronic version for color representation.*

These statistical analyses thus reveal that, in support of the theoretical insights described above, resonance periods are characterized by (1) high-amplitude, slowly propagating waves and (2) persistent, and therefore extreme, surface weather.

4.4. CONCLUSIONS AND DISCUSSIONS

Boreal summer circulation has seen pronounced changes over the last decades, trends which seem to have amplified since the onset of rapid Arctic amplification around 2000. Especially the reduction in EKE, but also in zonal mean flow, have created conditions favorable for the buildup of heat and drought conditions over the continents. Moreover, a cluster of resonance events is observed since 2000, which has increased the occurrence-frequency of high-amplitude quasi-stationary waves with wave numbers close to 7. This generally implies a weakening of transient synoptic eddy activity and more-frequent states of quasi-stationary flow. The intimate links between quasi-stationary forced waves and transient synoptic eddies [*Chang et al.*, 2002] are not addressed here, but it seems reasonable to assume that a reduction in fast-wave activity will favor the occurrence of quasi-stationary flow. In fact, *Horton et al.* report significant increasing trends in anticyclonic summer circulation over the eastern United States, Europe, and western Asia since 1979 [*Horton et al.*, 2015]. Blocking high-pressure anticyclones are occurring more often and also persist longer in these regions [*Horton et al.*, 2015]. As stated above, these regions are directly influenced by the North Atlantic storm track and thus weakening EKE is likely to favor anticyclonic flow here. In any case, these different detected changes in observed large-scale summer circulation strongly point toward more-persistent flow patterns and therefore more extreme surface weather. This is also consistent with the dramatic increase in heat extremes in Europe and some other midlatitude regions [*Coumou et al.*, 2013; *Coumou and Robinson*, 2013; *Russo et al.*, 2014; *Christidis et al.*, 2014]. Also climate models project these trends in boreal summer circulation to continue under future high-emission scenarios [*Lehmann et al.*, 2014].

The underlying drivers behind these circulation changes are currently less well understood although they are generally consistent with theories and numerical model experiments involving Arctic change [*Francis and Vavrus*, 2012; *Cvijanovic and Caldeira,* 2015; *Schneider et al.*, 2014; *Petrie et al.*, 2015 ; also see Chapter 2]. The classical way to attribute drivers behind observed changes involves numerical modeling experiments with either in- or excluding certain forcing components [*Screen et al.*, 2013; *Trenberth et al.*, 2014; *Cvijanovic and Caldeira*, 2015]. Though certainly a lot can be learned this way, it has been shown that current GCMs appear deficient in simulating near stationary Rossby wave patterns during summer [*Schubert et al.*, 2011; *Overland et al.*, 2012]. A supplementary approach would be to apply recently developed causal-discovery algorithms [*Runge et al.*, 2012, 2014] to disentangle the contributions from different drivers in observational and climate model data. Such methods can detect and quantify causal interactions and they have successfully been applied to disentangle causality in ocean circulation [*Schleussner et al.*, 2014] and atmospheric circulation in the tropics [*Runge et al.*, 2014].

Most recent studies on trends in persistent circulation and extreme events have focused on boreal winter circulation [*Cohen et al.*, 2014; *Walsh*, 2014]. In this season, recent Arctic amplification has been strongest [*Cohen et al.*, 2014] and also possible tropical drivers are thought to be much more important [*Trenberth et al.*, 2014] (see Chapter 4 for tropical influences). Irrespective of these possible far-away drivers, the equator-to-pole temperature gradient in the midlatitudes has seen the most pronounced changes in boreal summer [*Coumou et al.*, 2015]. Further, due to its smaller year-to-year variability as compared to the other seasons, long-term trends in summer circulation are detectable at an earlier stage. But apart from that, the important physical mechanisms are likely to be quite different between warm and cold season. For example, in winter the variability in the polar night jet and sudden stratospheric warming events are thought to be important in forcing tropospheric circulation [*Baldwin and Dunkerton*, 2001; *Kim et al.*, 2014]. In summer such stratospheric interactions are unlikely to play a role. Clearly more research is needed to understand the differences between cold- and warm-season circulations including the drivers behind their variability. Much can be learned by analyzing possible resonance events in nonsummer seasons and also in the Southern Hemisphere. Due to its almost opposite nature in terms of land-ocean distribution, the Southern Hemisphere can be used to test different theories. For example, in boreal summer, double jet circulation patterns occur relatively frequently whereby the poleward jet forms around 70°N, that is, roughly at the boundary of the Arctic Ocean where a strong thermal contrast forms. Therefore, double jet patterns are somewhat unlikely in the Southern Hemisphere (although this remains to be tested) and this could thus provide insights in the relative role of double jets in triggering resonance events if the latter appear to exist in the Southern Hemisphere. Also long-term reanalysis, like the twentieth century reanalysis [*Compo et al.*, 2011], and climate models from the Coupled Climate Model Intercomparison Project [*Covey et al.*, 2003] should be analyzed for resonance events in both hemispheres. Key questions to address are whether climate models can actually reproduce such nonlinear wave dynamics and what the links

are with the typical modes of variability like the Arctic Oscillation or ENSO.

Atmosphere dynamical changes associated with long-term climate change are a key contributor to uncertainty in future climate model projections [*Shepherd*, 2014; *Bony et al.*, 2015]. Here we have highlighted the importance of atmospheric circulation in causing devastating extreme surface weather events throughout the Northern Hemisphere midlatitudes. To reduce uncertainty in climate model projections and assess future impacts from extreme weather, the underlying processes and drivers will need to be understood in much more detail.

ACKNOWLEDGMENTS

JL was supported by the German Research Foundation (DFG, CO994/2-1) and DC and KK were supported by the German Federal Ministry of Education and Research (BMBF, 01LN1304A).

REFERENCES

Alexander, L. (2010), Extreme heat rooted in dry soils, *Nat. Geosci.*, *4*, 12–13.

Baldwin, M. P., and T. J. Dunkerton (2001), Stratospheric harbingers of anomalous weather regimes, *Science*, *294*, 581–584.

Barriopedro, D., E. M. Fischer, J. Luterbacher, R. M. Trigo, and R. García-Herrera (2011), The hot summer of 2010: Redrawing the temperature record map of Europe, *Science*, *332*, 220–224.

Bony, S., B. Stevens, D. M. W. Frierson, C. Jakob, M. Kageyama, R. Pincus, T. G. Shepherd, S. C. Sherwood, A. P. Siebesma, A. H. Sobel, M. Watanabe, and M. J. Webb (2015), Clouds, circulation and climate sensitivity, *Nat. Geosci.*, *8*, 261–268.

Chang, E. K. M., S. Lee, and K. Swanson (2002), Storm track dynamics, *J. Climate*, *15*, 2163–2183.

Christidis, N., G. S. Jones, and P. Stott (2014), Dramatically increasing chance of extremely hot summers since the 2003 European heatwave, *Nature Climate Change*, *5*, 46–50.

Cohen, J., J Screen, J C Furtado, M Barlow, D Whittleston, D Coumou, J Francis, K Dethloff, D Entekhabi, J Overland, and J. Jones (2014), Recent Arctic amplification and extreme mid-latitude weather, *Nat. Geosci.*, *7*, 627–637.

Compo, G. P., J. S. Whitaker, P. D. Sardeshmukh, N. Matsui, R. J. Allan, X. Yin, B. E. Gleason, R. S. Vose, G. Rutledge, P. Bessemoulin, S. Brönnimann, M. Brunet, R. I. Crouthamel, A. N. Grant, P. Y. Groisman, P. D. Jones, M. C. Kruk, A. C. Kruger, G. J. Marshall, M. Maugeri, H. Y. Mok, Ø. Nordli, T. F. Ross, R. M. Trigo, X. L. Wang, S. D. Woodruff, and S. J. Worley (2011), The Twentieth Century Reanalysis Project, *Quart. J. Roy. Meteor. Soc.*, *137*, 1–28.

Coumou, D., and A. Robinson (2013), Historic and future increase in the global land area affected by monthly heat extremes, *Environ. Res. Lett.*, *8*, 1–6.

Coumou, D., and S. Rahmstorf (2012), A decade of weather extremes, *Nature Climate Change*, *2*, 491–496.

Coumou, D., A. Robinson, and S. Rahmstorf (2013), Global increase in record-breaking monthly-mean temperatures, *Climate Change*, *118*, 771–782.

Coumou, D., J. Lehmann, and J. Beckmann (2015), The weakening summer circulation in the Northern Hemisphere mid-latitudes, *Science*, *348*, 324–327.

Coumou, D.,V. Petoukhov, and A. V. Eliseev (2011), Three-dimensional parameterizations of the synoptic scale kinetic energy and momentum flux in the Earth's atmosphere, *Nonlinear Process. Geophys.*, *18*, 807–827.

Coumou, D., V. Petoukhov, S. Rahmstorf, S. Petri, and H. J. Schellnhuber (2014), Quasi-resonant circulation regimes and hemispheric synchronization of extreme weather in boreal summer, *Proc. Natl. Acad. Sci. USA*, *111*, 12331–12336.

Covey, C., K. M. Achutarao, U. Cubasch, P. Jones, S. J. Lambert, M. E. Mann, T. J. Phillips, and K. E. Taylor (2003), An overview of results from the Coupled Model Intercomparison Project, *Global Planet. Change*, *37*, 103–133.

Cowtan, K., and R. G. Way (2013), Coverage bias in the HadCRUT4 temperature series and its impact on recent temperature trends, *Quart. J. Roy. Meteor. Soc.*, *133*, 459–477.

Cvijanovic, I., and K. Caldeira (2015), Atmospheric impacts of sea ice decline in CO2 induced global warming, *Climate Dyn., 44* (5–6); doi: 10.1007/s00382-015-2489-1.

Dee, D. P., S. M. Uppala, A. J. Simmons, P. Berrisford, P. Poli, S. Kobayashi, U. Andrae, M. A. Balmaseda, G. Balsamo, P. Bauer, P. Bechtold, A. C. M. Beljaars, L. van de Berg, J. Bidlot, N. Bormann, C. Delsol, R. Dragani, M. Fuentes, A. J. Geer, L. Haimberger, S. B. Healy, H. Hersbach, E. V.. Hólm, L. Isaksen, P. Kållberg, M. Köhler, M. Matricardi, A. P. McNally, B. M. Monge-Sanz, J-J. Morcrette, B-K. Park, C. Peubey, P. de Rosnay, C. Tavolato, J-N. Thépaut, and F. Vitart (2011), The ERA-interim reanalysis: Configuration and performance of the data assimilation system, *Quart. J. Roy. Meteor. Soc.*, *137*, 553–597.

Dole, R., M. Hoerling, J. Perlwitz, J. Eischeid, P. Pegion, T. Zhang, X. W. Quan, T. Xu, and D. Murray (2011), Was there a basis for anticipating the 2010 Russian heat wave?, *Geophys. Res. Lett.*, *38*.

Francis, J., and S. J. Vavrus (2015), Evidence for a wavier jet stream in response to rapid Arctic warming, *Environ. Res. Lett*., *10* ; Online: http://stacks.iop.org/1748-9326/10/i=1/a=014005?key=crossref.74581076f734b2377ec8042d3aebe25d.

Francis, J. A., and S. J. Vavrus (2012), Evidence linking Arctic amplification to extreme weather in the mid-latitudes, *Geophys. Res. Lett.*, *39*, L06801.

Hong, C., H. Hsu, N. Lin, and H. Chiu (2011), Roles of European blocking and tropical-extratropical interaction in the 2010 Pakistan flooding, *Geophys. Res. Let.*, *38*, 6.

Horton, D. E., N. C. Johnson, D. Singh, D. L. Swain, B. Rajaratnam, and N. S. Diffenbaugh (2015), Contribution of changes in atmospheric circulation patterns to extreme temperature trends, *Nature*, *522*, 465–469.

Kalnay, E., M. Kanamitsu, R. Kistler, W. Collins, D. Deaven, L. Gandin, M. Iredell, S. Saha, G. White, J. Woollen, Y. Zhu, M. Chelliah, W. Ebisuzaki, W. Higgins, J. Janowiak, K. C. Mo, C. Ropelewski, J. Wang, A. Leetma, R. Reynolds, R. Jenne, and D. Joseph (1996), The NCEP/NCAR 40-year reanalysis project, *Bull. Amer. Meteor. Soc.*, 437–471.

Kim, B-M., S-W. Son, S-K. Min, J-H. Jeong, S-J. Kim, X. Zhang, T. Shim, and J-H. Yoon (2014), Weakening of the stratospheric polar vortex by Arctic sea-ice loss, *Nat. Commun.*, *5*, 4646.

Kyselý, J. (2008), Influence of the persistence of circulation patterns on warm and cold temperature anomalies in Europe: Analysis over the 20th century, *Global Planet. Change*, *62*, 147–63.

Kyselý, J., and R. Huth (2005), Changes in atmospheric circulation over Europe detected by objective and subjective methods, *Theor. App. Climatol.*, *85*, 19–36.

Lau, W. K. M., and K-M. Kim (2012), The 2010 Pakistan flood and Russian heat wave: Teleconnection of hydrometeorological extremes, *J. Hydrometeor.*, *13*, 392–403

Lehmann, J., and D. Coumou (2015), The influence of mid-latitude storm tracks on hot, cold, dry, and wet extremes, *Sci. Rep.*, *5*, 1–9.

Lehmann, J., D. Coumou, K. Frieler, A. V. Eliseev, and A. Levermann (2014), Future changes in extratropical storm tracks and baroclinicity under climate change, *Environ. Res. Lett.*, *9*, 084002.

Mueller, B., and S. I. Seneviratne (2012), Hot days induced by precipitation deficits at the global scale, *Proc. Nat. Acad. Sci. USA*, *109*, 12398–12403.

O'Gorman, P. A. (2010), Understanding the varied response of the extratropical storm tracks to climate change, *Proc. Nat. Acad. Sci. USA*, *107*, 19176–19180.

Overland, J. E., J. A. Francis, E. Hanna, and M. Wang (2012), The recent shift in early summer Arctic atmospheric circulation, *Geophys. Res. Lett.*, *39*, L19804.

Palmer, T. (2014), Record-breaking winters and global climate change, *Science*, *344*, 803–804.

Pedlosky, J. (1979), *Geophysical Fluid Dynamics*, Springer, New York.

Petoukhov, V., S. Rahmstorf, S. Petri, and H. J. Schellnhuber (2013), Quasiresonant amplification of planetary waves and recent Northern Hemisphere weather extremes., *Proc. Nat. Acad. Sci. USA*, *110*, 5336–5341.

Petrie, R. E., L. C. Shaffrey, and R. T. Sutton (2015), Atmospheric response in summer linked to recent Arctic sea ice loss, *Quart. J. Roy. Meteor. Soc.*, *141*, 2070–2076.

Rahmstorf, S., and D. Coumou (2011), Increase of extreme events in a warming world, *Proc. Natl. Acad. Sci. USA*., *108*, 17905–17909.

Runge, J., J. Heitzig, N. Marwan, and J. Kurths (2012), Quantifying causal coupling strength: A lag-specific measure for multivariate time series related to transfer entropy, *Phys. Rev. E*, *86*, 061121.

Runge, J., V. Petoukhov, and J. Kurths (2014), Quantifying the strength and delay of climatic interactions: The ambiguities of cross correlation and a novel measure based on graphical models, *J. Climate*, *27*, 720–739.

Russo, S., A. Dosio, R. G. Graversen, J. Sillmann, H. Carrao, M. B. Dunbar, A. Singleton, P. Montagna, P. Barbosa, and J. V. Vogt (2014), Magnitude of extreme heat waves in present climate and their projection in a warming world, *J. Geophys. Res. Atmos.*, *119*, 12,500–12,512.

Schär, C., P. L. Vidale, D. Lüthi, C. Frei, C. Häberli, M. A. Liniger, and C. Appenzeller (2004), The role of increasing temperature variability in European summer heatwaves, *Nature*, *427*, 332–336.

Schleussner, C. F., J. Runge, J. Lehmann, and A. Levermann (2014), The role of the North Atlantic overturning and deep ocean for multi-decadal global-mean-temperature variability, *Earth Syst. Dyn.*, *5*, 103–115.

Schneider, T., T. Bischoff, and H. Plotka (2014), Physics of changes in synoptic midlatitude temperature variability, *J. Climate*, *28* (6); doi: 10.1175/JCLI-D-14-00632.1.

Schneidereit, A., S. Schubert, P. Vargin, F. Lunkeit, X. Zhu, D. H. W. Peters, and K. Fraedrich (2012), Large-scale flow and the long-lasting blocking high over Russia: Summer 2010, *Monthly Weather Rev.*, *140*, 2967–2981.

Schubert, S., H. Wang, and M. Suarez (2011), Warm season subseasonal variability and climate extremes in the Northern Hemisphere: The role of stationary Rossby waves, *J. Climate*, *24*, 4773–4792.

Schubert, S. D., H. Wang, R. D. Koster, M. J. Suarez, and P. Y. Groisman (2014), Northern Eurasian heat waves and droughts, *J. Climate*, *27*, 3169–3207.

Screen, J. A., and I. Simmonds (2014), Amplified mid-latitude planetary waves favour particular regional weather extremes, *Nature Climate Change*, *4*, 704–709.

Screen, J. A., I. Simmonds, C. Deser, and R. Tomas (2013), The atmospheric response to three decades of observed Arctic sea ice loss, *J. Climate*, *26*, 1230–1248.

Shepherd, T. G. (2014), Atmospheric circulation as a source of uncertainty in climate change projections, *Nat. Geosci.*, *7*, 703–708.

Tachibana, Y., T. Nakamura, H. Komiya, and M. Takahashi (2010), Abrupt evolution of the summer Northern Hemisphere annular mode and its association with blocking, *J. Geophys. Res.*, *115*, 13.

Trenberth, K. E., J. T. Fasullo, G. Branstator, and A. S. Phillips (2014), Seasonal aspects of the recent pause in surface warming, *Nature Climate Change*, *4*, 911–916.

Walsh, J. E. (2014), Intensified warming of the Arctic: Causes and impacts on middle latitudes, *Glob. Planet. Change*, *117*, 52–63.

Wang, S. Y., L. E. Hipps, R. R. Gillies, X. Jiang, and A. L. Moller (2010), Circumglobal teleconnection and early summer rainfall in the US intermountain west, *Theor. App. Climatol.*, *102*, 245–252.

Wang, S. Y., R. E. Davies, and R. R. Gillies (2013), Identification of extreme precipitation threat across midlatitude regions based on short-wave circulations, *J. Geophys. Res. Atmos.*, *118*, 11059–11074.

Woollings, T., and M. Blackburn (2012), The North Atlantic jet stream under climate change and its relation to the NAO and EA patterns, *J. Climate*, *25*, 886–902.